Gap-filling states induced by disorder and Zeeman coupling in the nodeless chiral superconducting Bi/Ni bilayer system

Rasoul Ghadimi, Mehdi Kargarian,* and S. Akbar Jafari
Department of Physics, Sharif University of Technology, Tehran 14588-89694, Iran

(Received 28 March 2019; published 8 July 2019)

Motivated by the recently discovered time-reversal symmetry-breaking superconductivity in the epitaxial Bi/Ni bilayer system with transition temperature $T_c \approx 4.2$ K and the observation of a zero-bias anomaly in a background of gap-filling states in tunneling measurements, we show that gap-filling states can appear in the fully gapped $d_{xy} \pm id_{x^2-y^2}$ superconducting states. We consider a model of helical electron states with d-wave pairing. In particular, we show that both magnetic and nonmagnetic impurities can create states within the superconducting gap. Alternatively, we show that the coupling of the electron spins to the in-plane Zeeman field provided by nickel can also create gap-filling states by producing Bogoliubov Fermi surfaces.

DOI: 10.1103/PhysRevB.100.024502

I. INTRODUCTION

The interplay between topology and electronic band structures in insulators, superconductors, and metals has received enormous attention and interest in recent years and has become a central issue in condensed-matter physics [1–3]. The nontrivial topology encoded in the bulk band structures, usually characterized by integer numbers, results in nontrivial consequences for the electronic states living on the boundary of the system: the topologically protected gapless surface states. Helical edge states at the one-dimensional boundary of HgTe [4,5], Dirac electrons on the surface of the three-dimensional topological materials Bi_2Se_3 and Bi_2Te_3 [6,7], Majorana fermions at the open ends of a one-dimensional topological superconductor [8], and the Fermi arcs in topological Weyl semimetals [9] such as TaAs [10–12] are a few known examples.

Special attention has been paid to the realization of topological superconductors promising a platform for topological quantum computations [13], a central paradigm in building a quantum computer. At the heart of material realization lies the nontrivial pairing wave function of Cooper pairs of electrons in the vicinity of the Fermi surface. While the phonon-based mechanism for superconductivity leads to the conventional s-wave superconductor, the intrinsic spin or charge density fluctuations due to electron correlations may result in a more complex structure for the pairing wave functions [14,15], for instance, in cuprates, Sr_2RuO_4 [16,17], and UPt_3 [18]. Alternatively, the nontrivial pairings can be induced by an ingenious combination of more conventional materials. A famously celebrated structure was introduced by Fu and Kane in Ref. [19], where a conventional s-wave superconductor proximitized to the surface of topological insulators (sSc-TI interface) was shown to support Majorana zero-energy states in vortex cores. Furthermore, the surface of topological insulators can be replaced with a more conventional two-dimensional electron gas with strong Rashba spin-orbit coupling, where the spin degeneracy is lifted, and a magnetic field or a Zeeman coupling turns the conventional induced s-wave pairing into a topological superconductor [20,21].

The recently discovered superconductivity with rather high critical temperature $T_c \approx 4.2$ K in an epitaxial Bi/Ni bilayer system [22] provided yet another example of a superconducting state with nontrivial pairing. The bilayer system is schematically shown in Fig. 1, where the surface termination Bi(110) is exposed to vacuum and Ni is a ferromagnet with in-plane magnetization. The optical measurements of the Kerr signal from the Bi(110) surface clearly show that the superconductivity breaks the time-reversal symmetry (TRS) [23]. Not only that, cooling below T_c in a weak magnetic field applied to the sample and measuring resistivity on warming up in the zero field show that the pairing states must break the TRS *spontaneously*. The theoretical model proposed in Ref. [23] uses the dominantly spin-orbit coupled electronic states localized on the surface of Bi(110), showing that the pairing symmetry should be $d_{xy} \pm id_{x^2-y^2}$, a chiral topological superconductor characterized by Chern numbers $c = \pm 2$. The complex structure of the superconducting order parameter indicates that the superconductivity in the Bi/Ni system is fully gapped, an observation which is in agreement with the recently measured optical conductivity using time-domain terahertz spectroscopy [24].

In addition to the transport and optical measurements outlined above, a zero-bias anomaly on a background of gap-filling states has also been observed in the point-contact Andreev reflection [22]. The gap-filling states seemingly contradict a fully gapped $d_{xy} \pm id_{x^2-y^2}$ superconductor. Understanding the origin of the gap-filling states is the main motivation of our work in this paper. We ask the following specific question: do the gap-filling states arise in topological $d_{xy} \pm id_{x^2-y^2}$ superconductors? We give an affirmative answer to this question by introducing two possible scenarios. These states may appear as a result of (i) magnetic and nonmagnetic

*kargarian@physics.sharif.edu

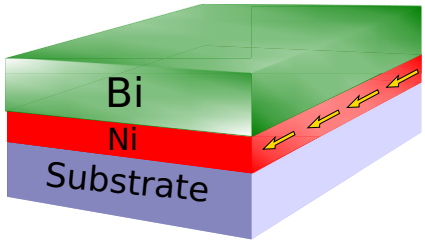

FIG. 1. Schematic representation of the epitaxial Bi/Ni bilayer system grown on a substrate such as MgO. The arrows show the in-plane magnetization of Ni.

impurities distributed randomly through the system and/or (ii) emergent Bogolon Fermi surfaces due to the coupling of electron spins to in-plane magnetic moments shown by arrows in Fig. 1. In the first scenario we treat the disorder effects using the Abrikosov-Grokov formalism [25] and ignore the inhomogeneity which might result in enhancement of superconductivity [26–30]. In particular, we show that there is a critical disorder strength beyond which the gap closes. Impurity bound states may arise in chiral superconductors in the absence of spin-orbit coupling [31] and also in systems with extrinsically induced superconductivity [32]. In our work we consider intrinsically chiral superconductors in systems with strong spin-orbit coupling.

The second scenario was first introduced for the sSc-TI interface, where it is found that the gapless states appear in the presence of Zeeman coupling [33]. We extend this finding to the chiral superconductors which may be relevant to the superconducting states in the Bi/Ni system, although the zero-bias anomaly requires careful treatment of Andreev bound states localized between the domains with opposite $d_{xy} \pm id_{x^2-y^2}$ chiralities [23] and we leave it for future study. Assuming bulk superconductivity [24] with possible nodal p-wave pairing [34], an analysis based on the Andreev bound states was developed [35] as a possible origin of the zero-bias anomaly.

This paper is organized as follows. We first discuss the disorder-induced states in Sec II, and then the effects of in-plane Zeeman coupling are discussed in Sec III. Section IV concludes.

II. DISORDER-INDUCED GAP-FILLING STATES IN CHIRAL SUPERCONDUCTORS

The chiral $d_{xy} \pm id_{x^2-y^2}$ superconductors are fully gapped. However, the point-contact Andreev reflection measurements show that below the critical temperature some states appear within the gap, the gap-filling states, with a notable zero-bias anomaly [22]. Here our aim is to understand the gap-filling states by considering a minimal model, which can describe the chiral superconducting states in the clean limit, in the presence of magnetic and nonmagnetic impurities. The electron states at the Bi(110) surface are strongly spin momentum locked due to the breaking of inversion symmetry near the surface [36] with a large hole pocket located around the center of the surface Brillouin zone. The latter pocket resembles the helical states at the surface of topological insulators. Notice that the bulk Bi is not a topological insulator, so there are also other small electron and hole pockets at the surface of Bi, and the helical spin structure is merely an effect of strong Rashba coupling [36]. However, for simplicity of formalism, below we first begin with the large hole pocket, the one similar to the surface of a topological insulator, in Sec. II A. Then multiple Fermi surfaces are studied in Sec. II B by considering a two-dimensional (2D) electron gas in the presence of Rashba spin-orbit coupling. We also assume that the magnetic fluctuations of Ni provide the pairing glue, as detailed in Ref. [23]. Our objective is to study the effects of disorder on the superconducting states.

A. Surface of a topological insulator

The effective description of the surface states of topological insulators is given by the 2D Hamiltonian $\boldsymbol{\sigma} \times \mathbf{k} \cdot \hat{z}$, where $\mathbf{k} = (k_x, k_y)$ is the wave vector and $\boldsymbol{\sigma} = (\sigma_x, \sigma_y)$ are Pauli matrices [1]. After a rotation it can be brought to the canonical Dirac form $\boldsymbol{\sigma} \cdot \mathbf{k}$, or, equivalently,

$$H_0' = \sum_{\mathbf{k},\sigma\sigma'} c^\dagger_{\mathbf{k}\sigma}[v_F|\mathbf{k}|(\sin\theta_\mathbf{k}\sigma_y + \cos\theta_\mathbf{k}\sigma_x) - \mu]_{\sigma\sigma'}c_{\mathbf{k}\sigma'}, \quad (1)$$

where $\theta_\mathbf{k}$ is the polar angle of $\mathbf{k}$ plus $\pi/2$. This Hamiltonian can be diagonalized by the following transformation:

$$d^\dagger_{\mathbf{k}\lambda} = \frac{1}{\sqrt{2}}(c^\dagger_{\mathbf{k}\uparrow} + \lambda e^{i\theta_\mathbf{k}} c^\dagger_{\mathbf{k}\downarrow}), \quad (2)$$

where $\lambda = \pm$ is helicity and labels the energy bands. Motivated by earlier work on the TRS breaking superconductivity in the Bi/Ni system and the theoretical proposal of $d \pm id$ pairing in this system [23], we formulate the effect of impurity scattering for such a superconducting state. Using the time-reversal (TR) operator $\Theta = i\sigma_y\mathcal{K}$, with $\mathcal{K}$ being the complex conjugation operator, the TR transformation of the creation operator $d^\dagger_{\mathbf{k}\lambda}$ becomes $\tilde{d}^\dagger_{\mathbf{k}\lambda} = \Theta d^\dagger_{\mathbf{k}\lambda}\Theta^{-1} = \lambda e^{-i\theta_\mathbf{k}} d^\dagger_{-\mathbf{k}\lambda}$, which can be used to construct the pairing interaction from the time-reversed partners as

$$H_{sc} = \sum_\mathbf{k} \Delta e^{-i2\theta_\mathbf{k}} d^\dagger_{\mathbf{k}+}\tilde{d}^\dagger_{\mathbf{k}+} + \text{H.c.} \quad (3)$$

We have included only the pairing between electron states with positive helicity, which is justified when the chemical potential is much larger than the pairing energy scale, i.e., the paring Hamiltonian is projected on the Fermi surface. In terms of the Nambu spinor $\psi_\mathbf{k} = (d_{\mathbf{k}+}, \tilde{d}^\dagger_{\mathbf{k}+})^T$ we can write the superconducting Hamiltonian as

$$H_0 = \sum_\mathbf{k} \psi^\dagger_\mathbf{k}[(v_F|\mathbf{k}| - \mu)\tau_3 + \Delta\cos 2\theta_\mathbf{k}\tau_1 + \Delta\sin 2\theta_\mathbf{k}\tau_2]\psi_\mathbf{k}, \quad (4)$$

where Pauli matrices τ act within the particle-hole space. On top of this clean pairing Hamiltonian we add a disorder term H_{dis}. The total Hamiltonian becomes

$$H = H_0 + H_{\text{dis}}, \quad (5)$$

where

$$H_{\text{dis}} = \sum_{i=1}^{N_{\text{dis}}} \sum_\sigma c^\dagger_{i\sigma}(\mu_i\delta_{\sigma\sigma'} + J\mathbf{S}_i \cdot \boldsymbol{\sigma}_{\sigma\sigma'})c_{i\sigma'}, \quad (6)$$

which describes scattering from magnetic and nonmagnetic impurities. For the latter the random scalar potential is given by the random variables μ_i, while the randomness in the magnetic impurities is given by the random orientation of the local spin $\mathbf{S}_i$. The exchange coupling J is essentially determined by the hybridization of conduction and impurity electron states and the strength of the on-site Hubbard term, which is assumed to be nonrandom. The average values of μ_i and $\mathbf{S}_i$ vanish, but their standard deviations are nonzero and together with the concentration of impurities determine the strength of impurity interactions.

By Fourier transform to momentum space $H_{\rm dis}$ becomes

$$H_{\rm dis} = \frac{1}{\mathcal{A}} \sum_{i,\sigma,\mathbf{k}\mathbf{k}'} e^{-i(\mathbf{k}-\mathbf{k}')\cdot\mathbf{R}_i} c^\dagger_{\mathbf{k}\sigma} (\mu_i \delta_{\sigma\sigma'} + J\mathbf{S}_i \cdot \boldsymbol{\sigma}_{\sigma\sigma'}) c_{\mathbf{k}'\sigma},$$

where $\mathcal{A}$ is the area of the system. In the band basis it takes the following form:

$$H_{\rm dis} = \frac{1}{2\mathcal{A}} \sum_{i,\lambda\lambda',\mathbf{k}\mathbf{k}'} d^\dagger_{\mathbf{k}\lambda} \bar{\mathcal{H}}_{\rm dis}(\mathbf{k},\mathbf{k}') d_{\mathbf{k}'\lambda'}, \tag{7}$$

with

$$\bar{\mathcal{H}}_{\rm dis}(\mathbf{k},\mathbf{k}') = e^{-i(\mathbf{k}-\mathbf{k}')\cdot\mathbf{R}_i} \left(\mu_i v^{\mathbf{k},\mathbf{k}'}_{\lambda,\lambda'} + J\mathbf{S}_i \cdot \mathbf{m}^{\mathbf{k},\mathbf{k}'}_{\lambda,\lambda}\right), \tag{8}$$

where

$$\begin{aligned} v^{\mathbf{k},\mathbf{k}'}_{\lambda,\lambda'} &\equiv 1 + \lambda\lambda' e^{-i\theta_{\mathbf{k}} + i\theta_{\mathbf{k}'}}, \\ \left(\mathbf{m}^{\mathbf{k},\mathbf{k}'}_{\lambda,\lambda'}\right)_x &\equiv \lambda e^{-i\theta_{\mathbf{k}}} + \lambda' e^{i\theta_{\mathbf{k}'}}, \\ \left(\mathbf{m}^{\mathbf{k},\mathbf{k}'}_{\lambda,\lambda'}\right)_y &\equiv i\lambda e^{-i\theta_{\mathbf{k}}} - i\lambda' e^{i\theta_{\mathbf{k}'}}, \\ \left(\mathbf{m}^{\mathbf{k},\mathbf{k}'}_{\lambda,\lambda'}\right)_z &\equiv 1 - \lambda\lambda' e^{-i\theta_{\mathbf{k}} + i\theta_{\mathbf{k}'}}. \end{aligned}$$

The above Hamiltonian is compactly represented in Nambu space as

$$H_{\rm dis} = \frac{1}{2\mathcal{A}} \sum_{i,\mathbf{k}\mathbf{k}'} \psi^\dagger_{\mathbf{k}} \mathcal{H}_{\rm dis}(\mathbf{k},\mathbf{k}') \psi_{\mathbf{k}'}, \tag{9}$$

where

$$\mathcal{H}_{\rm dis}(\mathbf{k},\mathbf{k}') = e^{-i(\mathbf{k}-\mathbf{k}')\cdot\mathbf{R}_i} (\mu_i V^{\mathbf{k},\mathbf{k}'} + J\mathbf{S}_i \cdot \mathbf{M}^{\mathbf{k},\mathbf{k}'}). \tag{10}$$

Here by assumption of a large, positive chemical potential we focus on $\lambda = +1$ matrix elements, i.e.,

$$V^{\mathbf{k},\mathbf{k}'} = \begin{pmatrix} v^{\mathbf{k},\mathbf{k}'}_{++} & 0 \\ 0 & \tilde{v}^{\mathbf{k},\mathbf{k}'}_{+,+} \end{pmatrix}, \tag{11}$$

$$\mathbf{M}^{\mathbf{k},\mathbf{k}'} = \begin{pmatrix} \mathbf{m}^{\mathbf{k},\mathbf{k}'}_{++} & 0 \\ 0 & \tilde{\mathbf{m}}^{\mathbf{k},\mathbf{k}'}_{++} \end{pmatrix}, \tag{12}$$

where we have introduced

$$\begin{aligned} \tilde{v}^{\mathbf{k},\mathbf{k}'}_{\lambda,\lambda'} &= (-\lambda\lambda' e^{-i\theta_{\mathbf{k}} + i\theta_{\mathbf{k}'}}) v^{-\mathbf{k}',-\mathbf{k}}_{\lambda',\lambda}, \\ \tilde{\mathbf{m}}^{\mathbf{k},\mathbf{k}'}_{\lambda,\lambda'} &\equiv -\lambda\lambda' e^{-i\theta_{\mathbf{k}} + i\theta_{\mathbf{k}'}} \mathbf{m}^{-\mathbf{k}',-\mathbf{k}}_{\lambda',\lambda}. \end{aligned}$$

In order to study the effect of disorder, we use the language of Green's functions. The disordered and clean Green's functions are defined as $G(\mathbf{k}, i\omega_n) = (i\omega_n - H)^{-1}$ and $G^{(0)}(i\omega_n) = (i\omega_n - H_0)^{-1}$, respectively, where ω_n is the fermionic Matsubara frequency. According to Dyson's equation, these Green's functions are related by

$$G(\mathbf{k}, i\omega_n)^{-1} = G^{(0)}(\mathbf{k}, i\omega_n)^{-1} - \Sigma(\mathbf{k}, i\omega_n), \tag{13}$$

where, in the self-consistent Born approximation up to second order, the self-energy is given by [33,37]

$$\Sigma(\mathbf{k}, i\omega_n) \approx \langle \mathcal{H}_{\rm dis}(\mathbf{k},\mathbf{k}) \rangle + \sum_{\mathbf{k}'} \langle \mathcal{H}_{\rm dis}(\mathbf{k},\mathbf{k}') G(\mathbf{k}', i\omega_n) \mathcal{H}_{\rm dis}(\mathbf{k}',\mathbf{k}) \rangle, \tag{14}$$

where $\langle \cdots \rangle$ means that the ensemble average is taken over disorder configurations. Following the approach presented in Refs. [32,38] for disordered systems, we assume that the excitations can be described in terms of an effective, clean single-particle Hamiltonian $\tilde{H}_0$, which is similar to the original H_0 with Δ now depending on ω_n; that is, we make the following replacement: $\Delta \to \Delta_n$ in H_0. Similarly, for the Green's function the spectral rearrangements due to disorder are taken into account by $i\omega_n \to i\tilde{\omega}_n$, where $i\tilde{\omega}_n$ is a function of $i\omega_n$, as described below. The effective Hamiltonian $\tilde{H}_0$ satisfies $G(i\omega_n) = (i\tilde{\omega}_n - \tilde{H}_0)^{-1}$. Equations (13) and (14) can now be cast into an algebraic self-consistency between $i\tilde{\omega}_n$ and Δ_n [see Eqs. (17) and (18)].

Since we have assumed that the mean values of μ_i and $\mathbf{S}_i$ are zero, the first term in Eq. (14) vanishes. However, the standard deviations are [37]

$$\frac{1}{\mathcal{A}} \langle \mu_i \mu_j e^{-i\mathbf{q}\cdot R_i} e^{-i\mathbf{q}'\cdot R_j} \rangle_{\rm dis} = n_{\rm dis} \bar{\mu^2} \delta_{i,j} \delta_{\mathbf{q},\mathbf{q}'}, \tag{15}$$

$$\frac{1}{\mathcal{A}} \langle S^\alpha_i S^\beta_j e^{-i\mathbf{q}\cdot R_i} e^{i\mathbf{q}'\cdot R_j} \rangle_{\rm dis} = \frac{1}{3} n_{\rm dis} S(S+1) \delta_{ij} \delta_{\alpha\beta} \delta_{\mathbf{q}+\mathbf{q}',0}, \tag{16}$$

where $n_{\rm dis}$ is the disorder concentration and S is the value of the spin of the magnetic impurity.

Obviously, there is no correlation between electrostatic and magnetic scattering forces, i.e., $\langle \mu_i \mathbf{S}_j \rangle = 0$. Therefore, the nonzero contribution of the second term in Eq. (14) arises from the above fluctuations. By assumption of a constant density of states (DOS) $N(0)$ at the Fermi surface the integral in the second term of Eq. (14) can be performed, giving rise to the following equations for $i\tilde{\omega}_n$ and Δ_n:

$$\tilde{\omega}_n = \omega_n + \Gamma \frac{\tilde{\omega}_n}{2\sqrt{\tilde{\Delta}_n^2 + \tilde{\omega}_n^2}}, \tag{17}$$

$$\tilde{\Delta}_n = \Delta + \alpha\Gamma \frac{\tilde{\Delta}_n}{2\sqrt{\tilde{\Delta}_n^2 + \tilde{\omega}_n^2}}, \tag{18}$$

where $\Gamma = [\bar{u^2} + S(S+1)J^2]\pi n_{\rm dis} N(0)$ defines the disorder strength. Note that the assumption of constant $N(0)$ around the Fermi level is justified for parabolic bands as well as a highly doped Dirac cone.

For a chiral $d \pm id$ superconductor, $\alpha = 0$. This is because the $e^{2i\theta_{\mathbf{k}}}$ factors in the pairing enforce the angular integration becoming zero. Therefore, in the $d \pm id$ case, the pairing potential $\tilde{\Delta}_n$ is not renormalized in the presence of disorder, in sharp contrast to s-wave pairing. For the latter pairing and within a model that scatters only single particles (not the Cooper pairs), $\alpha = +1$ [38] (-1 [32]) for nonmagnetic (magnetic) disorders. This leads to an important difference between the chiral $d \pm id$ and s-wave pairings. In the s-wave case, the fact that $\tilde{\Delta}_n$ depends on n implies that for magnetic impurities ($\alpha = -1$) T_c will be suppressed much faster than that of nonmagnetic impurities ($\alpha = +1$). In the chiral $d \pm id$

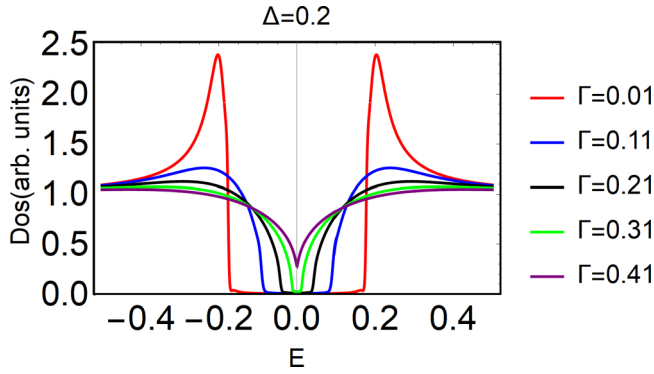

FIG. 2. Density of states as a function of energy for different disorder strengths Γ by $d+id$ superconductivity with amplitude $\Delta = 0.2$, showing the spectral gap closing with increasing disorder strength.

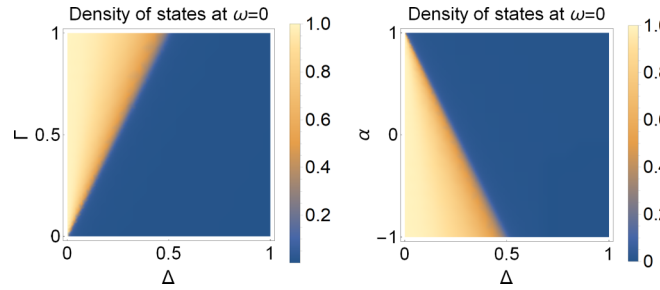

FIG. 3. Left: Density plot of $\omega = 0$ density of states in terms of disorder and pairing potential strength. Right: Map of the DOS at $\omega = 0$ for relatively large disorder strength $\Gamma = 0.5$ in the plane of α and Δ. $\alpha = 0$ corresponds to chiral superconductivity, while $\alpha = +1$ ($\alpha = -1$) corresponds to an s-wave superconductor with nonmagnetic (magnetic) scatterers.

case, α is always zero, and to that extent, the magnetic and nonmagnetic impurities have comparable effects on the T_c. As a function of impurity concentration, the transition temperature reads [32,38]

$$T_c(n_i) = T_c(0) - \frac{\pi}{8}(1-\alpha)\Gamma. \tag{19}$$

Therefore, the chiral superconductivity is fragile against impurity scattering, irrespective of the magnetic nature of scattering centers.

The DOS can be evaluated by momentum integration along with an analytical continuation $i\omega_n \to \omega + i0^+$ of the Green's function, and the expression reads

$$N(\omega) = -\frac{1}{\pi}N(0)\mathrm{Im}\left[\lim_{i\omega_n\to\omega+i0^+}\frac{-i\tilde{\omega}_n}{\sqrt{\tilde{\omega}_n^2+\Delta^2}}\right]. \tag{20}$$

One way to perform the analytical continuation is to use the Padé approximation to represent $-i\tilde{\omega}_n/\sqrt{\tilde{\omega}_n^2+\Delta^2}$ by the function $F(i\omega_n) = Q(i\omega_n)/P(i\omega_n)$, where Q and P are polynomials of $i\omega_n$, from which the analytical continuation $F(\omega + i0^+)$ can be evaluated. An alternative way is to perform the analytical continuation before solving the self-consistency Eqs. (17) and (18) [39]. We have checked that these two approaches give identical results.

In Fig. 2, we plot the DOS for $\Delta = 0.2$ as a function of energy for the different disorder strengths Γ indicated in the legend. It is seen that beyond a certain critical disorder strength the superconducting gap is completely filled and we have a gapless superconductor. The value of the DOS at $\omega = 0$ determines whether the superconductor is gapless or gapped. Therefore, in left panel of Fig. 3 we probe the density of states for $\omega \to 0$ in the plane of pairing and disorder strength. This gives us a border that separates gapless and gapped superconducting phases. To emphasize the difference between the behaviors of chiral and nonchiral superconductors against disorder, in the right panel of Fig. 3 for a fixed disorder strength of $\Gamma = 0.5$, we obtain a map of the DOS at $\omega = 0$ in the plane of α and Δ. The chiral superconductor corresponds to $\alpha = 0$. The s-wave superconductors with magnetic (nonmagnetic) scatterers correspond to $\alpha = -1$ ($\alpha = +1$). This comparison indicates that the impurity-induced states can fill up the gap in the chiral superconductor, providing a possible explanation for the observed in-gap features in the Bi/Ni system [22].

B. Electron gas with Rashba coupling

In this section we employ the methods used in the preceding section to study the effects of disorder on chiral superconductors in a system with multiple Fermi surfaces. For simplicity we consider a two-dimensional electron gas in the presence of strong Rashba spin-orbit coupling described by the following Hamiltonian:

$$H_0 = \sum_{\mathbf{k},\sigma\sigma'} c^\dagger_{\mathbf{k}\sigma} H_{\sigma\sigma'}(\mathbf{k}) c_{\mathbf{k}\sigma'}, \tag{21}$$

with

$$H_{\sigma\sigma'}(\mathbf{k}) = \frac{|\mathbf{k}|^2}{2m}\delta_{\sigma\sigma'} + [v_R|\mathbf{k}|(\sin\theta_{\mathbf{k}}\sigma_y + \cos\theta_{\mathbf{k}}\sigma_x) - \mu]_{\sigma\sigma'}, \tag{22}$$

where the spin-orbit coupling is expressed in the form of a velocity scale v_R to make it similar to the helical surface states considered in the preceding section. This Hamiltonian reduces to the helical Hamiltonian (1) upon the replacement $m \to \infty$ and $v_R \to v_F$. The pairing in the two cases is, however, different. In the helical metallic case for any chemical potential, there is only one Fermi contour. But in the Rashba spin-orbit coupled case, the spin-orbit coupling splits the degenerate electron gas into two Fermi contours. For a large enough chemical potential, the two spin-orbit split Fermi contours will have opposite helicities. Therefore, the pairing will include *both* helicities $\lambda = \pm 1$,

$$H_{sc} = \sum_{\mathbf{k},\lambda} \Delta_\lambda e^{-i2\theta_{\mathbf{k}}} d^\dagger_{\mathbf{k}\lambda}\tilde{d}^\dagger_{\mathbf{k}\lambda} + \mathrm{H.c.}, \tag{23}$$

which together with Eq. (21) yields the following superconducting Hamiltonian:

$$H = \sum_{\mathbf{k}\lambda}\psi^\dagger_{\mathbf{k}}\left(\frac{\sigma_0+\lambda\sigma_3}{2}\right)\Big[\left(\frac{|\mathbf{k}|^2}{2m}+\lambda v_R|\mathbf{k}|-\mu\right)\tau_3 + \Delta_\lambda(\cos 2\theta_{\mathbf{k}}\tau_1 + \sin 2\theta_{\mathbf{k}}\tau_2)\Big]\psi_{\mathbf{k}}, \tag{24}$$

where $\psi_{\mathbf{k}} = (d_{\mathbf{k}+}, \tilde{d}^\dagger_{\mathbf{k}+}, d_{\mathbf{k}-}, \tilde{d}^\dagger_{\mathbf{k}-})^T$ is the Nambu spinor.

The calculation follows the same steps as in the preceding section with the difference that, instead of one helicity ($\lambda = +$ for the surface of the TI), now we have both helicities $\lambda = \pm$, and hence, for the impurity Hamiltonians in Eqs. (9) and (10) the relevant matrices will be 4×4, which are given by

$$V^{\mathbf{k},\mathbf{k}'} = \begin{pmatrix} v_{++}^{\mathbf{k},\mathbf{k}'} & 0 & v_{+-}^{\mathbf{k},\mathbf{k}'} & 0 \\ 0 & \tilde{v}_{+,+}^{\mathbf{k},\mathbf{k}'} & 0 & \tilde{v}_{+,-}^{\mathbf{k},\mathbf{k}'} \\ v_{-+}^{\mathbf{k},\mathbf{k}'} & 0 & v_{--}^{\mathbf{k},\mathbf{k}'} & 0 \\ 0 & \tilde{v}_{-+}^{\mathbf{k},\mathbf{k}'} & 0 & \tilde{v}_{--}^{\mathbf{k},\mathbf{k}'} \end{pmatrix} \tag{25}$$

and

$$\mathbf{M}^{\mathbf{k},\mathbf{k}'} = \begin{pmatrix} \mathbf{m}_{++}^{\mathbf{k},\mathbf{k}'} & 0 & \mathbf{m}_{+-}^{\mathbf{k},\mathbf{k}'} & 0 \\ 0 & \tilde{\mathbf{m}}_{++}^{\mathbf{k},\mathbf{k}'} & 0 & \tilde{\mathbf{m}}_{+-}^{\mathbf{k},\mathbf{k}'} \\ \mathbf{m}_{-+}^{\mathbf{k},\mathbf{k}'} & 0 & \mathbf{m}_{--}^{\mathbf{k},\mathbf{k}'} & 0 \\ 0 & \tilde{\mathbf{m}}_{-+}^{\mathbf{k},\mathbf{k}'} & 0 & \tilde{\mathbf{m}}_{--}^{\mathbf{k},\mathbf{k}'} \end{pmatrix}. \tag{26}$$

For the chiral $d \pm id$ superconductor we obtain $\tilde{\Delta}_{\lambda,n} = \Delta_\lambda$ due to the vanishing angular integration of $e^{2i\theta_{\mathbf{k}}}$. That is, $\alpha = 0$ in Eq. (18), albeit with a new helicity index acquired due to two Fermi contours. The self-consistency equation corresponding to Eq. (17) will now become

$$\tilde{\omega}_n = \omega_n + \Gamma \left(\xi \frac{\tilde{\omega}_n}{2\sqrt{\tilde{\omega}_n^2 + \Delta_-^2}} + \frac{\tilde{\omega}_n}{2\sqrt{\tilde{\omega}_n^2 + \Delta_+^2}} \right), \tag{27}$$

where

$$N_\lambda(0) = \frac{m}{2\pi} \left(1 - \lambda \frac{v_R}{\sqrt{\frac{2\mu}{m} + v_R^2}} \right)$$

is the DOS for the Fermi contour with helicity λ and

$$\xi = \frac{N_-(0)}{N_+(0)} > 1.$$

In this case from Eq. (27) it follows that the total DOS is given by

$$N(\omega) = \frac{2}{\Gamma\pi} \mathrm{Im}[\lim_{i\omega_n \to \omega + i0^+} i(\tilde{\omega}_n - \omega_n)], \tag{28}$$

which again can be calculated either by Padé analytic continuation or the direct solution of the self-consistency equations slightly above the real-frequency axis [39]. Densities of states for different Δ_+/Δ_- ratios with $\Delta_+ = 0.2$ and $\xi = 1.2$ as a function of energy are plotted in Fig. 4 for different disorder strengths: $\Gamma = 0$ [Fig. 4(a)], $\Gamma = 0.05$ [Fig. 4(b)], $\Gamma = 0.1$ [Fig. 4(c)], and $\Gamma = 0.15$ [Fig. 4(d)]. In Fig. 4(a), where the disorder is zero, both gaps are clearly visible as two coherent peaks. Adding a small amount of disorder, in Fig. 4(b), the visible peaks are smeared out, and both gaps start to get filled. Indeed, within Eq. (27), if the DOSs at zero energy for two bands were the same ($\xi = 1$), then both gaps would evolve similarly. In the present case corresponding to $\xi = 1.2$, both gaps are filled almost in the same manner. In this way, the smaller of the two gaps will be filled first. This is what happens in Fig. 4(c), where the smaller gap is filled in, while the larger gap still survives. Finally, in Fig. 4(d), both gaps are

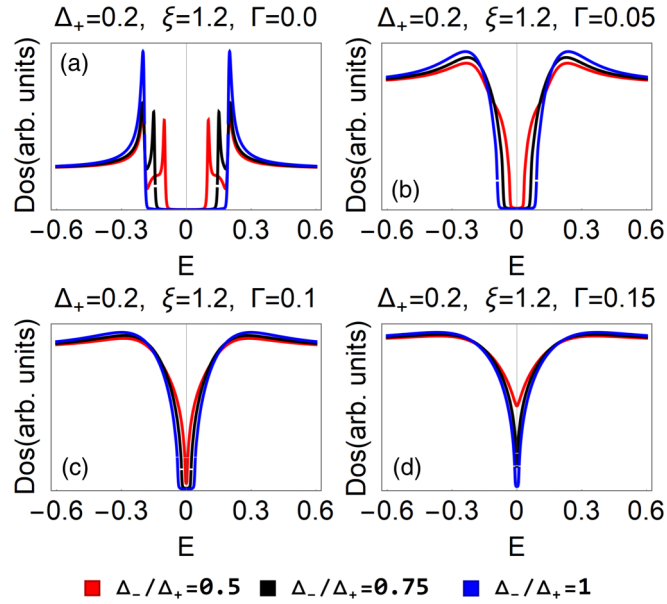

FIG. 4. Density of states for different Δ_-/Δ_+ ratios and $\xi = 1.2$ as a function of energy plotted for (a) $\Gamma = 0$, (b) $\Gamma = 0.05$, (c) $\Gamma = 0.1$, and (d) $\Gamma = 0.15$.

filled. Transport measurements can clearly indicate the value of Γ at which the smaller gap is filled. The second critical disorder at which the larger gap is filled shows up as a kink in the trend of the zero-bias peak as a function of disorder. The presence of such a kink is an essential difference between the chiral superconductivity in helical states and Rashba spin-orbit coupled systems. If the system is in a regime where the smaller gap is already filled, the specific heat measurement can detect the in-gap features and the larger gap.

III. GAP-FILLING STATES CAUSED BY IN-PLAIN ZEEMAN COUPLING

In this section we investigate the effect of in-plane magnetic field as another possible origin of midgap states. This mechanism was suggested recently [33] in the context of sSc-TI. In this section we investigate this mechanism for the chiral $d \pm id$ superconductivity and also for the d-wave pairings. In our setup shown in Fig. 1 the in-plane Zeeman coupling is provided by proximity to Ni. We start by adding an in-plane Zeeman field $V\sigma_y$ to Hamiltonian (21),

$$H_0 = \sum_{\mathbf{k}} c_{\mathbf{k}}^\dagger \left[\frac{|\mathbf{k}|^2}{2m}\sigma_0 + v_R(k_x\sigma_y - k_y\sigma_x) - \mu - V\sigma_y \right] c_{\mathbf{k}} + \sum_{\mathbf{k},\sigma\sigma'} (\Delta_{\sigma\sigma'}(\mathbf{k}) c_{\mathbf{k},\sigma}^\dagger c_{-\mathbf{k},\sigma'}^\dagger + \mathrm{H.c.}), \tag{29}$$

where the matrix $\Delta(\mathbf{k})$ is parameterized as follows:

$$\Delta(\mathbf{k}) = \begin{pmatrix} i|\mathbf{k}|\Delta_1(\mathbf{k})e^{-i\theta_{\mathbf{k}}} & \Delta_0(\mathbf{k}) \\ -\Delta_0(\mathbf{k}) & i|\mathbf{k}|\Delta_1(\mathbf{k})e^{i\theta_{\mathbf{k}}} \end{pmatrix}. \tag{30}$$

For numerical calculations we set $(m, v_R, \mu) = (0.3, 1, 0.5)$. To address the surface of the topological insulator we let $1/2m \to 0$ and $v_R = v_F$.

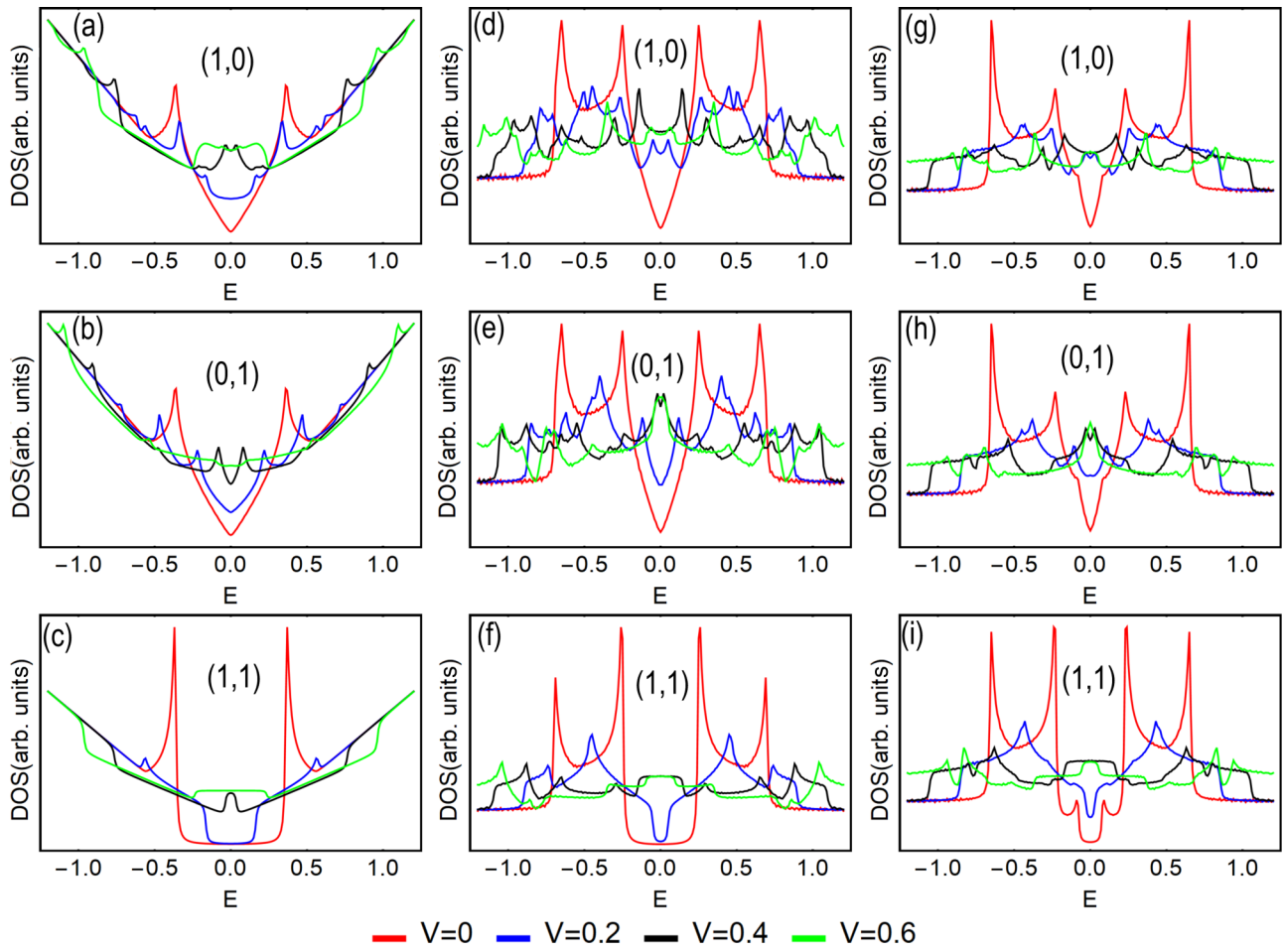

FIG. 5. Density of states for (a)–(c) the surface of the topological insulator and a Rashba electron gas with (d)–(f) spin singlet $(\Delta_0, \Delta_1) = (0.5, 0)$ and (g)–(i) spin triplet $(\Delta_0, \Delta_1) = (0, 0.5)$. The contribution of $d_{x^2-y^2}$ and d_{xy} pairings in each row is as follows: in the first row $(\zeta_{x^2-y^2}, \zeta_{xy}) = (1, 0)$. In the second row $(\zeta_{x^2-y^2}, \zeta_{xy}) = (0, 1)$, and in the third row we have set $(\zeta_{x^2-y^2}, \zeta_{xy}) = (1, 1)$, as shown in each panel. The values of in-plane Zeeman coupling V are indicated in the legend.

For the Rashba model with two Fermi contours $\lambda = \pm$ and, consequently, pairings $\Delta_\pm(\mathbf{k})$, the gap functions in Eq. (30) can be written as [40,41] $\Delta_1(\mathbf{k}) = \Delta_+(\mathbf{k}) - \Delta_-(\mathbf{k})$ and $\Delta_0(\mathbf{k}) = \Delta_+(\mathbf{k}) + \Delta_-(\mathbf{k})$. We take a general case for band pairings as $\Delta_\pm(\mathbf{k}) = (\Delta_0 \pm \Delta_1)(\zeta_{x^2-y^2}\cos 2\theta_\mathbf{k} + i\zeta_{xy}\sin 2\theta_\mathbf{k})$, where $(\zeta_{x^2-y^2}, \zeta_{xy})$ are $O(1)$ numerical parameters that encode the relative contribution of $d_{x^2-y^2}$ and d_{xy} pairings. With this identification for pairing functions, we rewrite the pairing matrix (30) as

$$\begin{pmatrix} i|\mathbf{k}|\Delta_1 e^{-i\theta_\mathbf{k}} & \Delta_0 \\ -\Delta_0 & i|\mathbf{k}|\Delta_1 e^{i\theta_\mathbf{k}} \end{pmatrix} (\zeta_{x^2-y^2}\cos 2\theta_\mathbf{k} + i\zeta_{xy}\sin 2\theta_\mathbf{k}), \tag{31}$$

where $(k_x, k_y) = |\mathbf{k}|(\cos\theta_\mathbf{k}, \sin\theta_\mathbf{k})$. In this way the explicit $d \pm id$ structure has been factored out. Now the amplitudes Δ_0 and Δ_1 do not depend on $\mathbf{k}$. The above pairing matrix has a structure in which the superconductivity is nodal unless both $\zeta_{x^2-y^2}$ and ζ_{xy} become nonzero, which then breaks the TRS.

In Fig. 5 we present DOSs for various cases. The three rows, from top to bottom, correspond to $(\zeta_{x^2-y^2}, \zeta_{xy}) = (1, 0)$, $(\zeta_{x^2-y^2}, \zeta_{xy}) = (0, 1)$, and $(\zeta_{x^2-y^2}, \zeta_{xy}) = (1, 1)$. The panels in the first column depict the results for the surface of topological insulators, while those in the next two columns are for the electron gas with Rashba coupling.

Let us first consider the surface of a topological insulator. As pointed out, in this case we need to set $\Delta_0 = \Delta_1 = 0.5$. The corresponding DOS is shown in Figs. 5(a)–5(c). Figures 5(a) and 5(b) correspond to nodal $d_{x^2-y^2}$ and d_{xy} pairing symmetries. As seen, in the absence of the Zeeman field we have a V-shaped pseudogap arising from the node in the pairing function, as shown by the solid red line. The smallest amount of in-plane Zeeman V gives rise to Bogoliubov Fermi contours, and consequently, a finite DOS is created at $E = 0$. The most interesting situation occurs when the superconducting state is fully gapped [Fig. 5(c)] due to TRS breaking of the $d_{x^2-y^2} + id_{xy}$ pairing wave function. In the absence of Zeeman coupling there is a clear gap in the DOS. However, a rather strong Zeeman coupling can fill the gap by creating Bogoliubov Fermi contours. The creation of the latter contours is shown in Fig. 6. In the normal case and in the absence of a Zeeman field the single Fermi contour is shown by a helical circle [Fig. 6(a)], emanating from the linear dispersion in Fig. 6(d). While in the chiral superconducting phase the Fermi contour disappears, an in-plane Zeeman field creates Bogoliubov Fermi contours [Fig. 6(b)], resulting from

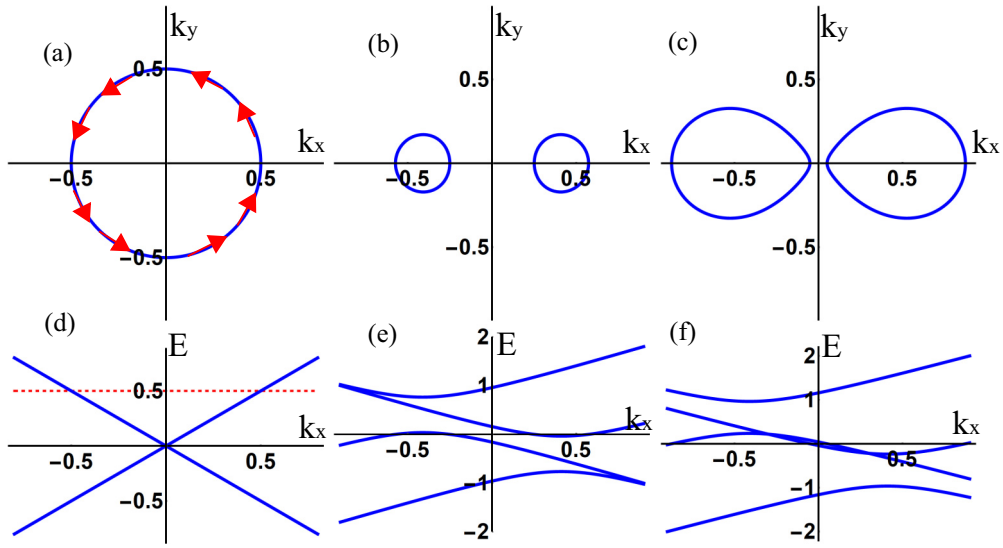

FIG. 6. (a) The Fermi contour and (d) the dispersion of the surface of the topological insulator. The red arrows indicate the helical structure of the Fermi contour, and the red dashed line indicates the Fermi level. Bogoliubov Fermi contours with $\Delta = 0.5$ appear for (b) $V = 0.4$ and (c) $V = 0.6$. (e) and (f) The corresponding Bogoliubov quasiparticle dispersions.

evolving the Bogoliubov quasiparticle bands and crossing the zero energy as shown in Fig. 6(e). A stronger Zeeman field makes the Bogoliubov Fermi contours more pronounced, as depicted in Figs. 6(c)–6(f).

The DOSs for the Rashba model are shown in Figs. 5(d)–5(g) for $d_{x^2-y^2}$ pairing, Figs. 5(e)–5(h) for d_{xy} pairing, and Figs. 5(f)–5(i) for $d_{x^2-y^2} + id_{xy}$ pairing. Here we can also tune Δ_0 and Δ_1 independently. We consider two extreme cases where $(\Delta_0, \Delta_1) = (0.5, 0)$, corresponding to purely singlet pairing, as shown in Figs. 5(d)–5(f), and $(\Delta_0, \Delta_1) = (0, 0.5)$, corresponding to a triplet case, as shown in Figs. 5(g)–5(i). Again, it is clearly seen that for nodal cases a tiny Zeeman field creates a finite DOS at zero energy, and the fully gapped case needs stronger Zeeman coupling for the gap to be filled with Bogoliubov quasiparticles.

IV. CONCLUSIONS

This work was mainly motivated by the observation of in-gap states in the point-contact tunneling measurements in the nodeless time-reversal symmetry-breaking superconducting epitaxial Bi/Ni bilayer system. In the previous work by one of the authors and coworkers [23], it was proposed that the pairing symmetry should be the surface chiral $d \pm id$ superconductor, in agreement with Kerr measurements and the thickness-dependent transition temperature. In this work we considered the effects of both magnetic and nonmagnetic impurities on the superconducting gap. We showed in all cases gap-filling states appear in the gap and start to fill it. Alternatively, we showed that the in-plane Zeeman coupling, which is produced by a Ni layer lying underneath Bi, can also create Bogoliubov Fermi contours of quasiparticles with nonvanishing spectral weight within the gap. This latter mechanism underlying the gap-filling states is of particular interest when we compare the value of the superconducting gap Δ with the strength of the Zeeman coupling V in the Bi/Ni bilayer. According to recent optical measurements, the value of the superconducting gap is $\Delta = 0.7$ mV [24], and the one for Zeeman coupling is $V = 2$ mV [34]. Thus, it is quite possible that the in-plane Zeeman coupling exceeding the gap creates Bogoliubov Fermi contours, and as we have shown in Figs. 5 and 6, a large number of gap-filling states appear.

It is interesting to examine the boundary modes localized between domains with opposite chiral pairings and their possible impact on the formation of the zero-bias anomaly observed in tunneling measurements, which we leave for future study.

ACKNOWLEDGMENTS

M.K. acknowledges the support from the Sharif University of Technology under Grant No. G690208. S.A.J. acknowledges Grant No. G960214 of the research deputy, Sharif University of Technology, and the support from Iran Science Elites Federation (ISEF).

[1] M. Z. Hasan and C. L. Kane, Rev. Mod. Phys. **82**, 3045 (2010).
[2] M. Z. Hasan and J. E. Moore, Annu. Rev. Condens. Matter Phys. **2**, 55 (2011).
[3] X.-L. Qi and S.-C. Zhang, Rev. Mod. Phys. **83**, 1057 (2011).
[4] B. A. Bernevig, T. L. Hughes, and S.-C. Zhang, Science **314**, 1757 (2006).
[5] M. König, S. Wiedmann, C. Brüne, A. Roth, H. Buhmann, L. W. Molenkamp, X.-L. Qi, and S.-C. Zhang, Science **318**, 766 (2007).
[6] H. Zhang, C.-X. Liu, X.-L. Qi, X. Dai, Z. Fang, and S.-C. Zhang, Nat. Phys. **5**, 438 (2009).
[7] Y. L. Chen, J. G. Analytis, J.-H. Chu, Z. K. Liu, S.-K. Mo, X. L. Qi, H. J. Zhang, D. H. Lu, X. Dai, Z. Fang, S. C. Zhang,

I. R. Fisher, Z. Hussain, and Z.-X. Shen, Science **325**, 178 (2009).
[8] A. Y. Kitaev, Phys. Usp. **44**, 131 (2001).
[9] X. Wan, A. M. Turner, A. Vishwanath, and S. Y. Savrasov, Phys. Rev. B **83**, 205101 (2011).
[10] B. Q. Lv, H. M. Weng, B. B. Fu, X. P. Wang, H. Miao, J. Ma, P. Richard, X. C. Huang, L. X. Zhao, G. F. Chen, Z. Fang, X. Dai, T. Qian, and H. Ding, Phys. Rev. X **5**, 031013 (2015).
[11] B. Q. Lv, N. Xu, H. M. Weng, J. Z. Ma, P. Richard, X. C. Huang, L. X. Zhao, G. F. Chen, C. E. Matt, F. Bisti, V. N. Strocov, J. Mesot, Z. Fang, X. Dai, T. Qian, M. Shi, and H. Ding, Nat. Phys. **11**, 724 (2015).
[12] S.-Y. Xu, I. Belopolski, N. Alidoust, M. Neupane, G. Bian, C. Zhang, R. Sankar, G. Chang, Z. Yuan, C.-C. Lee, S.-M. Huang, H. Zheng, J. Ma, D. S. Sanchez, B. Wang, A. Bansil, F. Chou, P. P. Shibayev, H. Lin, S. Jia, and M. Z. Hasan, Science **349**, 613 (2015).
[13] C. Nayak, S. H. Simon, A. Stern, M. Freedman, and S. Das Sarma, Rev. Mod. Phys. **80**, 1083 (2008).
[14] P. A. Lee, N. Nagaosa, and X.-G. Wen, Rev. Mod. Phys. **78**, 17 (2006).
[15] D. J. Scalapino, Rev. Mod. Phys. **84**, 1383 (2012).
[16] C. Kallin and J. Berlinsky, Rep. Prog. Phys. **79**, 054502 (2016).
[17] G. M. Luke, Y. Fudamoto, K. M. Kojima, M. I. Larkin, J. Merrin, B. Nachumi, Y. J. Uemura, Y. Maeno, Z. Q. Mao, Y. Mori, H. Nakamura, and M. Sigrist, Nature (London) **394**, 558 (1998).
[18] E. R. Schemm, W. J. Gannon, C. M. Wishne, W. P. Halperin, and A. Kapitulnik, Science **345**, 190 (2014).
[19] L. Fu and C. L. Kane, Phys. Rev. Lett. **100**, 096407 (2008).
[20] J. D. Sau, R. M. Lutchyn, S. Tewari, and S. Das Sarma, Phys. Rev. Lett. **104**, 040502 (2010).
[21] J. D. Sau, S. Tewari, R. M. Lutchyn, T. D. Stanescu, and S. Das Sarma, Phys. Rev. B **82**, 214509 (2010).
[22] X.-X. Gong, H.-X. Zhou, P.-C. Xu, D. Yue, K. Zhou, X.-F. Jin, H. Tian, G.-J. Zhao, and T.-Y. Chen, Chin. Phys. Lett. **32**, 067402 (2015).
[23] X. Gong, M. Kargarian, A. Stern, D. Yue, H. Zhou, X. Jin, V. M. Galitski, V. M. Yakovenko, and J. Xia, Sci. Adv. **3**, e1602579 (2017).
[24] P. Chauhan, F. Mahmood, D. Yue, P.-C. Xu, X. Jin, and N. P. Armitage, Phys. Rev. Lett. **122**, 017002 (2019).
[25] A. Abrikosov and L. Gor'Kov, Zh. Eksp. Teor. Fiz. **39**, 1781 (1960).
[26] B. M. Andersen, A. Melikyan, T. S. Nunner, and P. J. Hirschfeld, Phys. Rev. B **74**, 060501(R) (2006).
[27] M. N. Gastiasoro, P. J. Hirschfeld, and B. M. Andersen, Phys. Rev. B **88**, 220509(R) (2013).
[28] M. N. Gastiasoro and B. M. Andersen, Phys. Rev. B **98**, 184510 (2018).
[29] M. N. Gastiasoro, F. Bernardini, and B. M. Andersen, Phys. Rev. Lett. **117**, 257002 (2016).
[30] A. T. Rømer, S. Graser, T. S. Nunner, P. J. Hirschfeld, and B. M. Andersen, Phys. Rev. B **86**, 054507 (2012).
[31] M. Mashkoori, K. Björnson, and A. M. Black-Schaffer, Sci. Rep. **7**, 44107 (2017).
[32] I. Ozfidan, J. Han, and J. Maciejko, Phys. Rev. B **94**, 214510 (2016).
[33] N. F. Q. Yuan and L. Fu, Phys. Rev. B **97**, 115139 (2018).
[34] S.-P. Chao, Phys. Rev. B **99**, 064504 (2019).
[35] G. Zhao, X. Gong, J. He, J. Gifford, H. Zhou, Y. Chen, X. Jin, C. Chien, and T. Chen, arXiv:1810.10403.
[36] P. Hofmann, Prog. Surf. Sci. **81**, 191 (2006).
[37] H. Bruus and K. Flensberg, *Many-Body Quantum Theory in Condensed Matter Physics: An Introduction* (Oxford University Press, New York, 2004).
[38] Y. Ito, Y. Yamaji, and M. Imada, J. Phys. Soc. Jpn. **81**, 084707 (2012).
[39] M. Fathi and S. A. Jafari, Phys. B (Amsterdam, Neth.) **405**, 1658 (2010).
[40] K. V. Samokhin and V. P. Mineev, Phys. Rev. B **77**, 104520 (2008).
[41] R. Ghadimi, M. Kargarian, and S. A. Jafari, Phys. Rev. B **99**, 115122 (2019).